

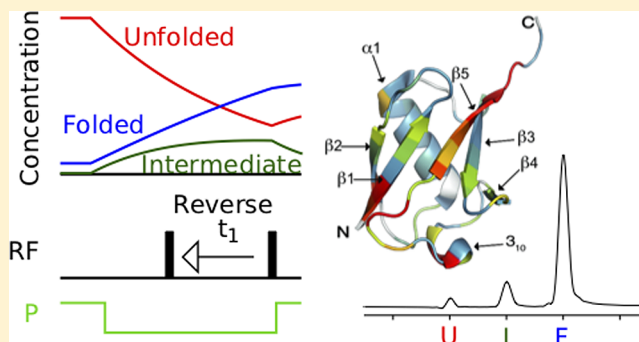
Interrupted Pressure-Jump NMR Experiments Reveal Resonances of On-Pathway Protein Folding Intermediate

Cyril Charlier,[‡] Joseph M. Courtney,[‡] Philip Anfinrud,[‡] and Ad Bax^{*†}

Laboratory of Chemical Physics, NIDDK, National Institutes of Health, Bethesda, Maryland 20892-0520, United States

Supporting Information

ABSTRACT: Previous pressure-jump NMR experiments on a pressure-sensitized double mutant of ubiquitin showed evidence that its folding occurs via two parallel, comparably efficient pathways: a single barrier and a two-barrier pathway. An interrupted folding NMR experiment is introduced, where for a brief period the pressure is dropped to atmospheric conditions (1 bar), followed by a jump back to high pressure for signal detection. Conventional, forward sampling of the indirect dimension during the low-pressure period correlates the ¹⁵N or ¹³C' chemical shifts of the unfolded protein at 1 bar to the ¹H frequencies of both the unfolded and folded proteins at high pressure. Remarkably, sampling the data of the same experiment in the reverse direction yields the frequencies of proteins present at the end of the low-pressure interval, which include unfolded, intermediate, and folded species. Although the folding intermediate ¹⁵N shifts differ strongly from natively folded protein, its ¹³C' chemical shifts, which are more sensitive probes for secondary structure, closely match those of the folded protein and indicate that the folding intermediate must have a structure that is quite similar to the native state.



INTRODUCTION

Proteins transition from their initially highly disordered to their well-defined native state on a time scale that is many orders of magnitude faster than would be expected from a random search of conformational space, pointing to the existence of pathways in this process.¹ For many small proteins, a single barrier on such pathways, separating the unfolded from the folded state, suffices to explain a large variety of experimental data, mostly derived from rapid mixing, stopped-flow experiments. It is now well-established that the actual barrier crossing event is exceedingly fast, diffusion-limited,^{2–5} and therefore difficult to observe directly. The presence of additional, lower barriers would result in short-lived intermediates, which would have low populations and be difficult to detect. NMR relaxation dispersion measurements, which are exquisitely sensitive for identifying such lowly populated states, have characterized a highly transient, on-pathway folding intermediate for a Fyn-SH3 mutant,^{6–8} suggesting that, perhaps, such intermediates are more prevalent than generally assumed. Most commonly, the protein folding process is probed by Trp fluorescence, fluorescence resonance energy transfer (FRET), or backbone amide hydrogen exchange.^{9–13} NMR spectroscopy has played an important role in these latter studies, yielding highly quantitative site-specific hydrogen exchange rates with a temporal resolution that is only limited by the speed at which the exchange process can be quenched.^{14–16} Such data yield the rates at which H-bonds form after initiation of the folding process. If differences

in the hydrogen exchange protection profiles are seen for various regions of the protein, these data point to the presence of folding intermediates, that is, multiple barriers on the folding pathway.^{17–19} In such work, NMR spectroscopy is used in an indirect manner, to probe the exchange-quenched sample at residue-specific resolution, and comparable results now also have become accessible by advances in mass spectrometry, thereby requiring much less sample.^{16,20,21}

Direct monitoring of protein folding by NMR is also possible, but due to the long time required to generate an NMR spectrum such studies initially were limited to slower folding or unfolding systems.^{22–25} However, improvements in technology about a decade ago have much increased the accessible time resolution.^{26,27}

In nonequilibrium folding experiments, experimental conditions are typically changed abruptly from those favoring the unfolded state to those favoring the native state. This may be accomplished by a sudden jump in pH, dilution of denaturant, release of a cofactor, or by a sudden drop in hydrostatic pressure. The latter method, switching the pressure, is particularly benign, allowing the protein to be probed under native buffer conditions. However, a prerequisite for pressure-induced unfolding is that the protein volume of the unfolded

Special Issue: William A. Eaton Festschrift

Received: August 30, 2018

Revised: September 21, 2018

Published: September 26, 2018

state is substantially lower than that of the folded state, in practice by at least ~ 50 mL/mol. Equilibrium NMR spectra, recorded as a function of pressure, typically over the 0.1–3 kbar range, then often permit the simultaneous observation of unfolded and folded protein resonances in a slow exchange equilibrium and can yield site-specific information on the state of each residue.^{28–32} Analogous to pressure-jump fluorescence experiments,³³ the temporal change in the NMR spectrum following a step change in pressure can reveal kinetic information, provided the kinetics are slower than the duration of the pressure change, which often represents a challenging requirement for NMR spectroscopy.^{25,34} Recently, this limitation has been addressed by the development of dedicated hardware that rapidly increases or decreases the pressure in the NMR sample cell in a manner synchronized with the data acquisition process.^{35,36} The ability to repeat the pressure-jump process thousands of times then provides access to processes on time scales much faster than those needed to collect an entire multidimensional NMR spectrum.^{26,36,37}

In our first application of the newly developed pressure-jump NMR hardware, we studied ubiquitin, sensitized to pressure by the introduction of two Val to Ala cavity-generating mutations (V17A and V26A), while retaining the same native structure as the wild-type protein.^{36,38} Below, this double mutant is referred to as VA2-ubiquitin. Ubiquitin has functioned as a model protein in numerous experimental and computational folding studies,^{27,39–49} and it is very well-suited for detailed NMR analyses, therefore providing a perfect system for technological and methodological developments. Prior work citing evidence for an intermediate in ubiquitin's folding pathway^{13,39,50} has been contested.⁵¹ Our work conclusively showed the presence of parallel, single-barrier, and double-barrier pathways, with their relative efficiency being a strong function of temperature.³⁶ A separate $C^{\delta 2}H_3$ signal for Leu-50 was transiently visible for the double-barrier intermediate,³⁶ and the average ^{15}N chemical shift during the folding process deviated from two-state behavior. This latter observation enabled estimation of the folding intermediate ^{15}N chemical shifts, which differed very substantially from those of both the unfolded and folded native states of the protein.⁵² Remarkably, the hydrogen exchange protection of the intermediate and native states was found to be very similar, with significantly delayed protection only observed for two residues in the folding intermediate.³⁸

Here, we demonstrate that direct observation of the ^{15}N and $^{13}C'$ chemical shifts of the folding intermediate becomes accessible by very minor modifications of a commonly used pulse scheme, where signals are digitized in a direction opposite to that conventionally used. For samples at equilibrium, the direction of sampling has no impact on the spectrum. In contrast, for the nonequilibrium, folding experiments, the forward and reverse sampled spectra are quite different. Significantly, reverse-sampled spectra yield chemical shifts of the folding intermediate that are the first step toward determining its detailed molecular structure.

RESULTS AND DISCUSSION

Forward Sampled Pressure-Jump HSQC and HNCO Pulse Schemes. The NMR resonance frequencies of both the folded and unfolded states of a protein are quite sensitive to hydrostatic pressure.^{30,53} Switching of the pressure during an NMR pulse scheme therefore is preferably performed during a period where the magnetization is stored along the z axis, such

that small fluctuations in the timing of the switching that are invariably associated with the mechanical movement of the valve have minimal effect on the observed signal. Many NMR pulse sequences have such periods built into them naturally and often utilize such delays to apply pulsed field gradients to remove spurious magnetization transfer pathways.^{54,55} For example, in the in-phase, composite-pulse-decoupled heteronuclear single quantum correlation (HSQC) experiment,⁵⁶ the intervals just after the first refocused insensitive nuclei enhanced by polarization transfer (INEPT) transfer of $^1H^N$ magnetization to ^{15}N , and prior to reverse INEPT transfer back to $^1H^N$, can be used for this purpose (Supporting Information, Figure 1A). A fully analogous scheme, which is essentially a two-dimensional (2D) version of the common HNCO experiment,⁵⁷ can be used to transfer magnetization from H_z to C'_zN_z , prior to generating transverse $^{13}C'$ magnetization by a 90° $^{13}C'$ pulse (Supporting Information Figure 1C). In our pressure-jump experiments, the pressure is dropped to 1 bar just after completing the first magnetization transfer from 1H to ^{15}N (for HSQC), or to C'_zN_z (for HNCO; Figure 1). We allow the folding to occur for a low-pressure

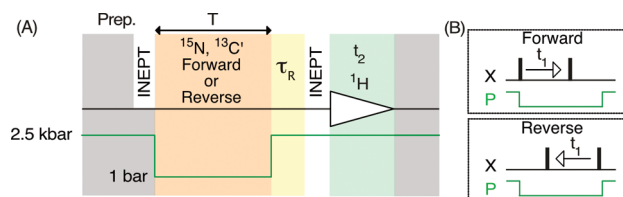


Figure 1. Simplified schematic of the forward and reverse detected pressure-jump 2D 1H – ^{15}N HSQC and 1H – $^{13}C'$ HNCO experiments. In both schemes, the spin system is prepared (Prep.) by a long (ca. 10 s) high-pressure protein denaturation interval, which is terminated by a refocused INEPT transfer to $^{15}N_z$ magnetization (HSQC) or to antiphase $^{13}C'_z$ $^{15}N_z$ magnetization (HNCO). During the subsequent low-pressure period (total duration T , ca. 70 ms) the ^{15}N (HSQC) or $^{13}C'$ (HNCO) frequency is encoded either in the regular, forward manner (B, top), or in the reverse manner (B, bottom), where the second ^{15}N (HSQC) or $^{13}C'$ (HNCO) pulse is always applied just prior to the jump back to high pressure, and the first pulse is moved stepwise to the left. Protein folding takes place during the low-pressure interval but is interrupted by the jump back to high pressure, prior to signal detection. A vibration decay delay (yellow, ~ 150 ms), where magnetization is stored along the z axis, precedes transfer of magnetization to 1H for detection during t_2 . Full details of the pulse sequence are provided in Supporting Information Figure S1.

duration T , during which ^{15}N or $^{13}C'$ chemical shift is encoded for a variable t_1 evolution period. When recorded in the usual, forward manner (Figure 1B, top), the signal intensity at the end of the low-pressure period, prior to reverse INEPT transfer to 1H , is proportional to

$$M_z(t_1) = [U]_0 \cos(\omega_x t_1) \exp(-R_2^U t_1) \quad (1)$$

where ω_x denotes the angular ^{15}N or $^{13}C'$ frequency of the unfolded protein, assuming no residual folded protein remains present at the end of the high-pressure preparation period. $[U]_0$ is the concentration of unfolded protein present at the start of the low-pressure period. R_2^U corresponds to the sum of the transverse relaxation rate of the unfolded species, R_2 , and the forward folding rates, $k_{U \rightarrow I}$ and $k_{U \rightarrow F}$, from the unfolded to the intermediate (two-barrier pathway) and from the unfolded to the folded state (single-barrier pathway), respectively.

Concentrations of the three species (plotted in Figure S2A), unfolded $[U(t)]$, intermediate $[I(t)]$, and folded $[F(t)]$, at time t after the pressure drop are given by

$$[U](t) = [U]_0 \exp(-k't) \quad (2a)$$

$$[I](t) = [U]_0 \left(\frac{k_{U \rightarrow I}}{-k' + k_{I \rightarrow F}} \right) [\exp(-k't) - \exp(-k_{I \rightarrow F}t)] \quad (2b)$$

$$[F](t) = [U]_0 - [U](t) - [I](t) \quad (2c)$$

with $k' = k_{U \rightarrow I} + k_{U \rightarrow F}$.

While a fraction of protein will fold after the switch to low pressure and will precess with a folded chemical shift for the remainder of the t_1 period, its signal will remain invisible in the HSQC spectrum, as any signal with zero intensity at $t_1 = 0$ will have an integral of zero in the resulting spectrum. Moreover, the transverse phase of magnetization of a protein that switches from unfolded to folded at time τ after the first 90° pulse accumulates a transverse phase $\omega_U \tau$ and will evolve for the remainder of t_1 with ω_F . At the end of the t_1 evolution period its phase will be $\omega_U \tau + \omega_F(t_1 - \tau)$, and signals from proteins that switched to the folded state at different values of τ therefore will destructively interfere with one another (unless $\omega_U \approx \omega_F$) and not contribute significantly to observed signal (Figures S2A and S3). The same applies for any folding intermediate signal. Note that weak signals of the intermediate state are visible in the noise-free simulations (Figure S3B,D) but result from proteins that refolded during the “padding delay” between the pressure drop and the actual start of t_1 evolution (ca. 5 ms), included in the simulations, but below the detection threshold in the experimental spectra. The final, forward-sampled spectrum therefore yields resonances that carry the unfolded ^{15}N frequency at 1 bar in the F_1 dimension of the final 2D spectrum, correlated to ^1H frequencies of both the unfolded and folded protein at high pressure in the F_2 dimension (Figure 2A and Figure S3B,D). Similarly, the forward-sampled 2D HNCQ spectrum shows $^{13}\text{C}'$ resonances of the unfolded protein at 1 bar (F_1 dimension) correlated to ^1H frequencies of the next residue for both the unfolded and folded protein at high pressure (Figure 3A). Note that the VA2-ubiquitin unfolding rate at room temperature is slow, and proteins that switch to the folded state during the low-pressure period have insufficient time to unfold prior to ^1H detection at high pressure (Figure S2A).

Reverse Sampled, Interrupted Folding HSQC and HNCQ Pulse Schemes. Simply by changing the timing of the pulses that generate the t_1 modulation, the same pulse schemes used above for detection of the unfolded ^{15}N and $^{13}\text{C}'$ resonances at 1 bar can be used for detecting folding intermediates: By sampling the t_1 evolution in the reverse direction (Figure 1B, bottom), starting from the end of the low-pressure interval, after folding intermediates and folded proteins have developed, their signals will modulate the observed spectrum (Figure S3F,H). If the folding intermediate were resistant to high pressure, such a signal would resonate at the ^1H frequency of the folding intermediate during the ^1H detection period (F_2 dimension). However, as was observed previously in the classic interrupted folding experiments of Kiefhaber,^{26,58} intermediates are commonly less stable than the folded state and rapidly revert to the unfolded state once conditions are switched back to denaturing, that is, high pressure. Therefore, the t_2 -detected ^1H signal of the I state is

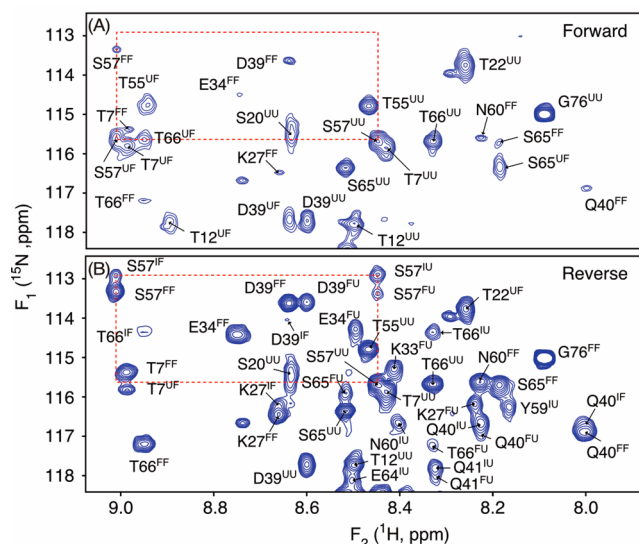


Figure 2. Small regions of the (A) forward and (B) reverse-sampled 2D ^1H – ^{15}N HSQC spectra of a sample containing $210 \mu\text{M}$ ^{15}N ubiquitin, pH 6.4. Full spectra are shown in Figures S5 and S6. Spectra are recorded at 600 MHz ^1H frequency, using a cryogenic probehead equipped with a z-axis pulsed field gradient accessory. The temperature was regulated at 25°C but drops by 3°C due to adiabatic expansion during the brief low-pressure period. The forward-recorded spectrum (A) primarily shows F_1 dimension correlations for species present at the start of the low-pressure period, that is, unfolded protein. These signals are correlated in the F_2 dimension with unfolded ^1H frequencies at 2.5 kbar for proteins that did not cross the folding barrier during the low-pressure period, or to folded ^1H frequencies at 2.5 kbar for proteins that crossed the folding barrier. The reverse-sampled spectrum (B) shows in the F_1 dimension the ^{15}N frequencies of all species present at the end of the low-pressure period, that is, unfolded, intermediate, and folded, correlated with their respective ^1H frequency at high pressure. Correlations are labeled by residue number, with the first superscript referring to the ^{15}N chemical shift of the unfolded (U), intermediate (I), or folded (F) state at the end of the low-pressure interval, and the second superscript denoting the state of the protein during detection. No I-state ^1H signals are observed, because the majority of I-state proteins revert to U prior to detection; an approximately twofold smaller fraction crosses the barrier to the folded state, yielding resonances superscripted IF. The pattern of correlations for S57 is marked by red dashed rectangles.

found at the high-pressure unfolded ^1H frequency (Figures 2B and 3B). For VA2-ubiquitin, we also find a minor fraction of I-state protein that switches to the native state prior to ^1H detection. This latter fraction gives rise to signals at the I-state ^{15}N frequency in the F_1 dimension (Figure S3H) and to the native-state, high-pressure ^1H frequency in the F_2 dimension. The intensity ratio of the I-state peaks, correlated to the unfolded and folded ^1H frequencies, corresponds to the ratio of the respective transition rates at high pressure $k_{I \rightarrow U}/k_{I \rightarrow F}$. The total amplitude of the folding intermediate signal I depends on the fraction of proteins that have switched to the intermediate state at time T after the drop to low pressure but have not progressed to the folded state (eq 2). The integrated peak intensity of a U, I, or F resonance of the reverse-sampled time domain corresponds to the time domain point sampled at $t_1 = 0$, that is, to the values $[U](T)$, $[I](T)$, and $[F](T)$, where T is the duration after the pressure drop at which the reverse sampling is started (Figure 1).

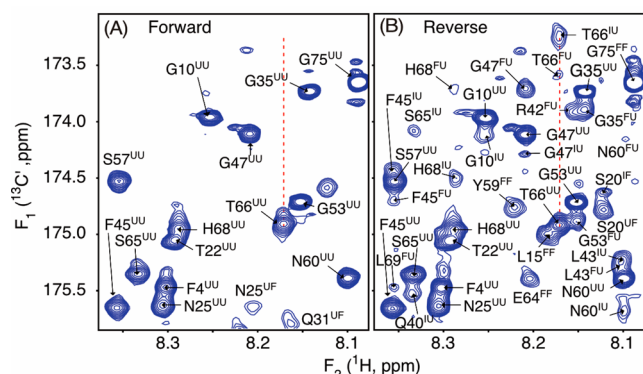


Figure 3. Small regions of the 600 MHz (A) forward and (B) reverse-sampled 2D ^1H – $^{13}\text{C}'$ HNCOSY spectra of a sample containing $125\ \mu\text{M}$ $^{15}\text{N}/^{13}\text{C}'/^2\text{H}$ -VA2-ubiquitin, pH 6.4, $25\ ^\circ\text{C}$. Full spectra are shown in Figures S7 and S8. Fully analogous to the spectra of Figure 2, the forward spectrum (A) primarily shows F_1 dimension correlations for unfolded protein, correlated to 2.5 kbar ^1H F_2 frequencies of either folded or unfolded protein. Analogously, the reverse-sampled spectrum (B) shows in the F_1 dimension the 1 bar $^{13}\text{C}'$ frequencies of U, I, and F species, correlated with 2.5 kbar ^1H frequency of the amide of the next residue. Each peak number indicates the residue that is $^{13}\text{C}'$ labeled, with the first superscript referring to the state of the protein during $^{13}\text{C}'$ evolution at 1 bar, and the second superscript denoting the state during ^1H detection at 2.5 kbar.

The decay profiles of the U-, I-, and F-state components with respect to t_1 are quite different from one another, with $[U](t_1)$ only being attenuated by true transverse relaxation, whereas $[I](t_1)$ and $[F](t_1)$ drop to zero at $t_1 = T$, even in the absence of transverse relaxation, since no intermediate or folded magnetization is present immediately after the pressure drop. Details are presented in Supporting Information Figure S2. The different, nonexponential decay profiles for the $[I](t_1)$ and $[F](t_1)$ components result in non-Lorentzian line shapes after Fourier transformation, with the I and F state resonances being broader than those of the U fraction that remains unfolded during the low-pressure period (Figure S3). The differences in line shapes require that integrated peak intensities be measured to obtain accurate concentrations of the U-, I-, and F-states of ubiquitin. These integrals cannot easily be measured because of the crowded spectra obtained in our study. Nevertheless, the spectra obtained by the reverse sampling method unambiguously reveal the ^{15}N and $^{13}\text{C}'$ frequencies of the intermediate state.

Comparison of the forward-sampled ^{15}N – ^1H HSQC (Figure 2A) with the reverse-sampled spectrum (Figure 2B) shows a multitude of new resonances in the latter. For example, the dashed red boxes outline correlations observed for residue S57. Each cross peak is marked by two superscripts, which refer to the state of the protein during t_1 evolution and during t_2 detection. For instance, the cross peak labeled S57^{IF} (top left in Figure 2B) corresponds to signal of the intermediate (I-state) ^{15}N frequency in the F_1 dimension, and the S57 ^1H frequency of the folded protein in the F_2 dimension. Note that the ^1H frequencies of the folded state at 2.5 kbar differ substantially from those at 1 bar but can easily be identified by recording a pressure-jump ^1H – ^{15}N 2D HSQC spectrum with preparation and ^{15}N evolution at 1 bar and ^1H detection at 2.5 kbar (Figure S4). Figure 2A shows two intense resonances, S57^{UF} and S57^{UU}, from proteins that were unfolded at the end of the preparation period (marked “Prep.” in Figure 1), and either

switched to the folded state during the low-pressure period (S57^{UF}) or remained unfolded (S57^{UU}). A very weak resonance, marked S57^{FF} (top left Figure 2A), corresponds to the small fraction ($\sim 6\%$) of proteins that remained folded at the end of the high-pressure preparation period. Because unfolding of the protein at high pressure is very slow, the corresponding S57^{FU} resonance has vanishing intensity. By contrast, the reverse-sampled spectrum (Figure 2B) shows a strong S57^{FF} peak with just above it a very weak S57^{IF} peak from the small fraction of proteins that were in the intermediate state at the end of the low-pressure period but crossed the barrier to the folded state prior to ^1H detection. A considerably stronger S57^{IU} resonance, at the same ^{15}N F_1 frequency, is observed for I-state proteins that switched back to the unfolded state prior to ^1H detection. The slow unfolding rate at high pressure causes only a very small ($\sim 10\%$) fraction of proteins that had reached the folded state at the end of the low-pressure period to revert back to the unfolded state, giving rise to a very weak S57^{FU} peak (Figure 2B). A stronger S57^{UU} resonance corresponds to proteins that remained unfolded during the low-pressure interval.

Measurement of I-State $^{13}\text{C}'$ Chemical Shifts. Fully analogous to the forward- and reverse-sampled ^{15}N – ^1H HSQC spectra, discussed above, the same forward and reverse sampling modes can be incorporated in the 2D HNCOSY pulse scheme (Supporting Information Figure S1C,D). The forward-sampled HNCOSY spectrum then shows correlations between the U-state $^{13}\text{C}'$ shift of residue i and the $^1\text{H}^{\text{N}}$ resonance of residue $i + 1$ in both the unfolded and folded states. For example, the dashed vertical line in Figure 3A, at the $^1\text{H}^{\text{N}}$ frequency of residue L67, shows a correlation to T66– $^{13}\text{C}'$. At the same frequency in the reverse-sampled spectrum (Figure 3B), the same T66^{IU} signal is observed, in addition to a correlation to the intermediate state, T66^{IU}, and a very weak resonance, T66^{FU}, from proteins that were folded at the end of the low-pressure interval but subsequently unfold during the ca. 150 ms high-pressure period that separated ^{15}N evolution from ^1H detection. Analogous T66^{FF} and T66^{IF} signals are present in the full spectrum, outside the region shown in Figure 3. Although the signal-to-noise ratio of the HNCOSY spectra is nearly twofold lower than for the HSQC spectra, recorded in a comparable amount of time, I-state $^{13}\text{C}'$ resonances could be identified with confidence for 70 of the potential 72 residues that are expected to give rise to such signals. Missing were $^{13}\text{C}'$ signals of three residues preceding a Pro, the C-terminal residue G76, as well as M1 due to rapid exchange of the amide of Q2, while resonance overlap precluded assignment of I23 and D52 in the crowded region of the reverse-sampled HNCOSY spectrum (Figure 3B; Figure S8).

Chemical Shift Characterization of the Folding Intermediate. The ^{15}N chemical shifts of the folding intermediate measured from the folding-interrupted HSQC spectrum agree closely with values obtained previously from the pseudo-three-dimensional (Ψ 3D) pressure-jump experiment (Figure 4), which measured the ensemble-averaged ^{15}N shift during the folding process by sampling a single time point in the indirect dimension (stroboscopic observation).⁵² The I-state frequency was then extracted by means of a fitting procedure.⁵² However, the stroboscopic measurement yielded relatively large uncertainties in the ensemble-averaged ^{15}N frequency of each residue, thereby adversely impacting the precision at which the frequency of the I-state component

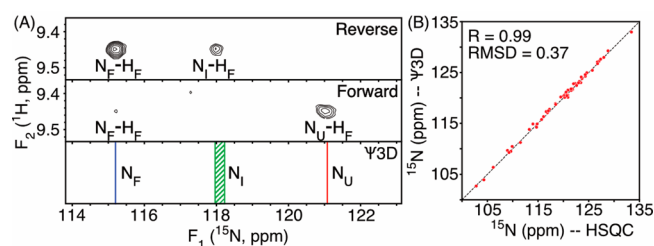


Figure 4. Comparison of spectral data of the E64 amide of VA2-ubiquitin, recorded with the pressure-jump 2D ^1H - ^{15}N HSQC experiment of Figure 1, and ^{15}N chemical shifts previously derived from stroboscopic observation of ^{15}N shifts in a Ψ 3D measurement.⁵² (A) ^{15}N F_1 strips taken at the E64 F_2 ^1H N frequency of folded ubiquitin at 2.5 kbar, with the bottom strip showing the results of previous fitting of the Ψ 3D data of this residue. (B) Correlation plot of the ^{15}N I-shifts extracted from the Ψ 3D spectrum (y -axis) with those of the reverse-sampled pressure-jump HSQC spectrum (x -axis). The Pearson correlation coefficient equals 0.99, with an RMSD of 0.37 ppm.

could be obtained. The current method yields highly precise peak positions but suffers from increased resonance overlap, as the number of resonances in the reverse-sampled, folding-interrupted spectra is threefold larger than that of the fully folded or fully unfolded protein. Consequently, the set of residues for which unambiguous I-state ^{15}N frequencies could be determined is somewhat smaller (59 vs 65 residues) than in the earlier work. With a root-mean-square difference (RMSD) of only 0.37 ppm (Figure 4B), agreement with the earlier measurement is very good, and results confirm that the I-state differs most from the F-state for the C-terminal strand, β 5, and its preceding loop, strand β 1, and the C-terminal residues of strand β 3, with β 5 being sandwiched between β 1 and β 3 in the natively folded state (Figure 5A,B).

^{15}N chemical shifts are exquisitely sensitive to a wide range of structural parameters, including H-bond strength, side-chain rotamer positioning, backbone torsion angles, and electrostatic effects from nearby charged groups,⁵⁹ complicating the interpretation of the ^{15}N chemical shift differences in structural terms. In contrast to ^{15}N , $^{13}\text{C}'$ chemical shifts correlate fairly well with protein secondary structure: $^{13}\text{C}'$ resonances in α -helical secondary structure are typically downfield-shifted by 2–3 ppm from random coil, whereas upfield (negative) secondary shifts of 1–2 ppm are typically observed in β -sheet. Using the reverse-sampled HNCO spectrum, we obtained a set of 70 $^{13}\text{C}'$ I-state chemical shifts (Figure 5C–E). The chemical shifts of the I-state reveal important new information on the secondary structure of this transient intermediate. Particularly striking is the closeness of the I-state $^{13}\text{C}'$ shifts to those of the folded state for residues F4–T55. Substantial chemical shift differences between the folded and intermediate states are observed for residues S57–L73, which correspond to the C-terminal β 5 strand, its preceding loop N60–S65, and the short 3_{10} helix preceding this loop. In addition, chemical shifts of residues Q2 and I3 in β 1 differ considerably between I- and F-states. The secondary $^{13}\text{C}'$ shifts of Q2 and I3 in the I-state are ca. -1.5 ppm, indicative of β -strand. Residues R72 and L73, which have close to random coil shifts in the native structure, show substantial negative and positive secondary shifts, respectively, in the I-state, indicative of well-defined structure for these residues. The chemical shift differences relative to the natively folded protein are mapped on a ribbon diagram of the folded structure (Figure 5E) and reveal more localized

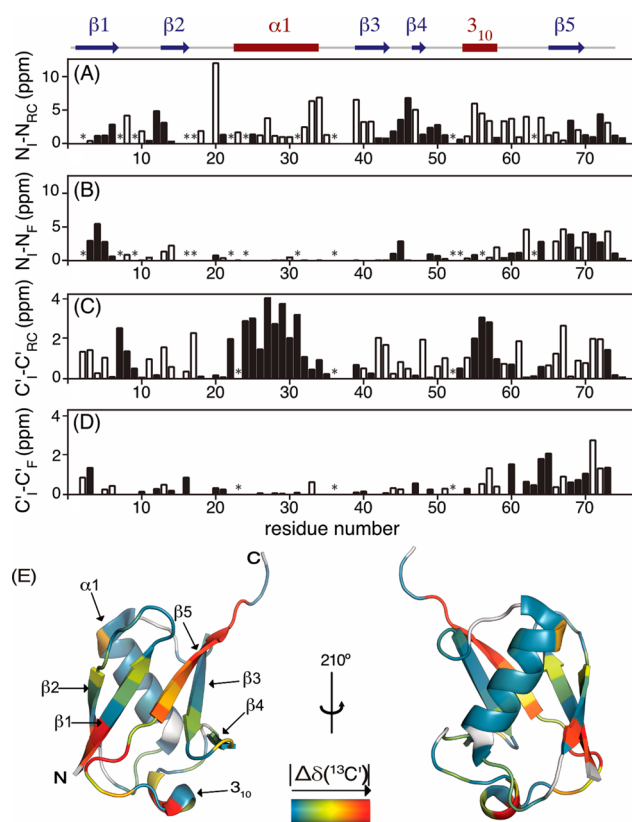


Figure 5. Comparison of 1 bar ^{15}N and $^{13}\text{C}'$ chemical shifts of the VA2-ubiquitin folding intermediate with those of the folded state (δ^{F}) and with random coil values (δ^{RC}) obtained with the program POTENCI.⁶³ Filled and open bars correspond to positive and negative values, respectively. (A) $\delta^{\text{I}}(^{15}\text{N}) - \delta^{\text{F}}(^{15}\text{N})$; (B) $\delta^{\text{I}}(^{15}\text{N}) - \delta^{\text{RC}}(^{15}\text{N})$; (C) $\delta^{\text{I}}(^{13}\text{C}') - \delta^{\text{F}}(^{13}\text{C}')$; (D) $\delta^{\text{I}}(^{13}\text{C}') - \delta^{\text{RC}}(^{13}\text{C}')$; (E) $|\Delta\delta(^{13}\text{C}')| = |\delta^{\text{I}}(^{13}\text{C}') - \delta^{\text{F}}(^{13}\text{C}')|$ color coded on a backbone ribbon structure of the native state of ubiquitin (PDB entry 2MJJB). Residues for which $|\Delta\delta(^{13}\text{C}')|$ could not be determined are shown in gray.

differences than previously seen from the ^{15}N chemical shift differences⁵² (Figure 5B). Strands β 3 and β 1 pair with the C-terminal strand in the native structure, and it therefore appears likely that any significant difference in the N60–S65 loop, which contains two reverse turns in the native structure, could propagate into β 5 and thereby β 1. A structural analysis, including the collection of pressure-jump nuclear Overhauser effect (NOE) data, currently in progress, will likely resolve the detailed structural differences between the intermediate and native states of the protein.

EXPERIMENTAL SECTION

Sample Preparation. ^{15}N - and ^{13}C - ^{15}N - ^2H -labeled VA2-ubiquitin was expressed and purified as described previously.³⁸ Importantly, a final high-performance liquid chromatography (HPLC) step was found necessary to prevent proteolysis at high pressure, where the denatured state of the protein is highly susceptible to proteolytic cleavage. Samples were dissolved in 25 mM potassium phosphate buffer, pH 6.4, using 1% D_2O for a field frequency lock.

NMR Spectroscopy. All NMR experiments were recorded on a Bruker 600 MHz spectrometer equipped with cryogenic probehead with a z -axis pulsed field gradient accessory. A 2.8 mm ID zirconia sample cell, rated for static pressures of up to 3 kbar (Daedalus, Inc.) was used.⁶⁰ The hardware enabling rapid

pressure switching, under control of the Bruker pulse program, has been described previously.³⁶ Both forward- and reverse-sampled pressure-jump HSQC spectra were recorded using a 210 μM uniformly ^{15}N -enriched sample of VA2-ubiquitin. The temperature was regulated at 25 $^{\circ}\text{C}$ during the high-pressure period, but it briefly drops by 3 $^{\circ}\text{C}$ during the low-pressure interval, which had a total duration of ca. 70 ms. The depressurization transition evolves approximately linear in time during the period in which fluid flow through the transfer tube is turbulent and transitions to a small exponential tail as the flow becomes laminar. Forward and reverse ^{15}N sampling was performed for a 60 ms interval, which was initiated ca. 5 ms after the pressure drop to avoid encroaching on the tail end of the pressure drop. Inversely, the reverse sampling is initiated ca. 3 ms prior to the switch to high pressure to avoid encroaching on the high-pressure transition, which occasionally experiences milliseconds timing jitter. A 150 ms delay separated the end of the low-pressure period from the reverse INEPT transfer of magnetization to ^1H for detection. This delay serves to let decay any mechanical vibrations in the system related to the pressure switches, which have their strongest impact on the high- γ ^1H signals. Spectra were recorded with four scans per free induction decay (FID), for a total of 120 complex t_1 increments per 2D spectrum. With a recycle delay of 9 s, the total measurement time per spectrum was ca. 2.5 h. For the forward- and reverse-sampled 2D HNCO spectra, 100 complex t_1 increments were sampled, with 16 scans per FID and a total measurement time of 8 h per spectrum, using a 125 μM uniformly $^{13}\text{C}/^{15}\text{N}/^2\text{H}$ -labeled sample.

All the NMR data were processed and analyzed using NMRPipe⁶¹ and NMRFAM-Sparky⁶² software.

■ ASSOCIATED CONTENT

Supporting Information

The Supporting Information is available free of charge on the ACS Publications website at DOI: 10.1021/acs.jpcc.8b08456.

Pressure-jump 2D pulse schemes, evolution of the concentration of the unfolded, intermediate, and folded species in a pressure-jump experiment, simulation of forward and reverse-sampled NMR data, pressure-jump HSQC spectra, intermediate chemical shifts of VA2-ubiquitin at 1 bar (PDF)

■ AUTHOR INFORMATION

Corresponding Author

*E-mail: bax@nih.gov.

ORCID

Philip Anfinrud: 0000-0002-8261-0624

Ad Bax: 0000-0002-9809-5700

Author Contributions

[‡]The manuscript was written through contributions of all authors. All authors have given approval to the final version of the manuscript. These authors contributed equally.

Notes

The authors declare no competing financial interest.

■ ACKNOWLEDGMENTS

We thank J. Ying, Y. Shen, and J. L. Baber, for technical support, and D. A. Torchia, T. R. Alderson, and G. M. Clore for useful discussions. This work was supported by the

Intramural Research Program of the National Institute of Diabetes and Digestive and Kidney Diseases.

■ REFERENCES

- (1) Dobson, C. M.; Sali, A.; Karplus, M. Protein folding: A perspective from theory and experiment. *Angew. Chem., Int. Ed.* **1998**, *37* (7), 868–893.
- (2) Cellmer, T.; Henry, E. R.; Hofrichter, J.; Eaton, W. A. Measuring internal friction of an ultrafast-folding protein. *Proc. Natl. Acad. Sci. U. S. A.* **2008**, *105* (47), 18320–18325.
- (3) Chung, H. S.; Louis, J. M.; Eaton, W. A. Experimental determination of upper bound for transition path times in protein folding from single-molecule photon-by-photon trajectories. *Proc. Natl. Acad. Sci. U. S. A.* **2009**, *106* (29), 11837–11844.
- (4) Chung, H. S.; Gopich, I. V.; McHale, K.; Cellmer, T.; Louis, J. M.; Eaton, W. A. Extracting Rate Coefficients from Single-Molecule Photon Trajectories and FRET Efficiency Histograms for a Fast-Folding Protein. *J. Phys. Chem. A* **2011**, *115* (16), 3642–3656.
- (5) Chung, H. S.; Eaton, W. A. Single-molecule fluorescence probes dynamics of barrier crossing. *Nature* **2013**, *502* (7473), 685–688.
- (6) Korzhnev, D. M.; Kay, L. E. Probing invisible, low-populated states of protein molecules by relaxation dispersion NMR spectroscopy: An application to protein folding. *Acc. Chem. Res.* **2008**, *41* (3), 442–451.
- (7) Korzhnev, D. M.; Neudecker, P.; Zarrine-Afsar, A.; Davidson, A. R.; Kay, L. E. Abp1p and fyn SH3 domains fold through similar low-populated intermediate states. *Biochemistry* **2006**, *45* (34), 10175–10183.
- (8) Bezsonova, I.; Korzhnev, D. M.; Prosser, R. S.; Forman-Kay, J. D.; Kay, L. E. Hydration and packing along the folding pathway of SH3 domains by pressure-dependent NMR. *Biochemistry* **2006**, *45* (15), 4711–4719.
- (9) Matouschek, A.; Kellis, J. T.; Serrano, L.; Fersht, A. R. Mapping the Transition-State and Pathway of Protein Folding by Protein Engineering. *Nature* **1989**, *340* (6229), 122–126.
- (10) Kim, P. S.; Baldwin, R. L. Intermediates in the folding reactions of small proteins. *Annu. Rev. Biochem.* **1990**, *59*, 631–660.
- (11) Bai, Y. W.; Sosnick, T. R.; Mayne, L.; Englander, S. W. Protein-Folding Intermediates - Native-State Hydrogen-Exchange. *Science* **1995**, *269* (5221), 192–197.
- (12) Schuler, B.; Lipman, E. A.; Eaton, W. A. Probing the free-energy surface for protein folding with single-molecule fluorescence spectroscopy. *Nature* **2002**, *419* (6908), 743–747.
- (13) Vallee-Belisle, A.; Michnick, S. W. Visualizing transient protein-folding intermediates by tryptophan-scanning mutagenesis. *Nat. Struct. Mol. Biol.* **2012**, *19* (7), 731–736.
- (14) Roder, H. Structural characterization of protein folding intermediates by proton magnetic resonance and hydrogen exchange. *Methods Enzymol.* **1989**, *176*, 446–473.
- (15) Englander, S. W.; Mayne, L. Protein Folding Studied Using Hydrogen-Exchange Labeling and 2-Dimensional Nmr. *Annu. Rev. Biophys. Biomol. Struct.* **1992**, *21*, 243–265.
- (16) Dyson, H. J.; Wright, P. E. How Does Your Protein Fold? Elucidating the Apomyoglobin Folding Pathway. *Acc. Chem. Res.* **2017**, *50* (1), 105–111.
- (17) Eliezer, D.; Yao, J.; Dyson, H. J.; Wright, P. E. Structural and dynamic characterization of partially folded states of apomyoglobin and implications for protein folding. *Nat. Struct. Biol.* **1998**, *18* (2), 148–155.
- (18) Krishna, M. M. G.; Maity, H.; Rumbley, J. N.; Englander, S. W. Branching in the sequential folding pathway of cytochrome c. *Protein Sci.* **2007**, *16* (9), 1946–1956.
- (19) Hollien, J.; Marqusee, S. Comparison of the folding processes of T-thermophilus and E-coli ribonucleases H. *J. Mol. Biol.* **2002**, *316* (2), 327–340.
- (20) Miranker, A.; Robinson, C. V.; Radford, S. E.; Aplin, R. T.; Dobson, C. M. Detection of Transient Protein-Folding Populations by Mass-Spectrometry. *Science* **1993**, *262* (5135), 896–900.

- (21) Hu, W. B.; Walters, B. T.; Kan, Z. Y.; Mayne, L.; Rosen, L. E.; Marqusee, S.; Englander, S. W. Stepwise protein folding at near amino acid resolution by hydrogen exchange and mass spectrometry. *Proc. Natl. Acad. Sci. U. S. A.* **2013**, *110* (19), 7684–7689.
- (22) Hoeltzli, S. D.; Frieden, C. Stopped-flow NMR spectroscopy - Real-time unfolding studies of 6-F19-tryptophan-labeled E. Coli dihydrofolate reductase. *Proc. Natl. Acad. Sci. U. S. A.* **1995**, *92* (20), 9318–9322.
- (23) Koide, S.; Dyson, H. J.; Wright, P. E. Characterization of a folding intermediate of apoplastocyanin trapped by proline isomerization. *Biochemistry* **1993**, *32* (46), 12299–12310.
- (24) Balbach, J.; Forge, V.; Vannuland, N. A. J.; Winder, S. L.; Hore, P. J.; Dobson, C. M. Following protein folding in real-time using NMR spectroscopy. *Nat. Struct. Biol.* **1995**, *2* (10), 865–870.
- (25) Roche, J.; Dellarole, M.; Caro, J. A.; Norberto, D. R.; Garcia, A. E.; Garcia-Moreno, B.; Roumestand, C.; Royer, C. A. Effect of Internal Cavities on Folding Rates and Routes Revealed by Real-Time Pressure-Jump NMR Spectroscopy. *J. Am. Chem. Soc.* **2013**, *135* (39), 14610–14618.
- (26) Schlepckow, K.; Wirmer, J.; Bachmann, A.; Kiefhaber, T.; Schwalbe, H. Conserved folding pathways of alpha-lactalbumin and lysozyme revealed by kinetic CD, fluorescence, NMR, and interrupted refolding experiments. *J. Mol. Biol.* **2008**, *378* (3), 686–698.
- (27) Schanda, P.; Forge, V.; Brutscher, B. Protein folding and unfolding studied at atomic resolution by fast two-dimensional NMR spectroscopy. *Proc. Natl. Acad. Sci. U. S. A.* **2007**, *104* (27), 11257–11262.
- (28) Royer, C. A.; Hinck, A. P.; Loh, S. N.; Prehoda, K. E.; Peng, X. D.; Jonas, J.; Markley, J. L. Effects of Amino-Acid Substitutions on the Pressure Denaturation of Staphylococcal Nuclease as Monitored by Fluorescence and Nuclear-Magnetic-Resonance Spectroscopy. *Biochemistry* **1993**, *32* (19), 5222–5232.
- (29) Yamaguchi, T.; Yamada, H.; Akasaka, K. Thermodynamics of Unfolding of Ribonuclease-a under High-Pressure - a Study by Proton Nmr. *J. Mol. Biol.* **1995**, *250* (5), 689–694.
- (30) Kitahara, R.; Hata, K.; Li, H.; Williamson, M. P.; Akasaka, K. Pressure-induced chemical shifts as probes for conformational fluctuations in proteins. *Prog. Nucl. Magn. Reson. Spectrosc.* **2013**, *71*, 35–58.
- (31) Urbauer, J. L.; Ehrhardt, M. R.; Bieber, R. J.; Flynn, P. F.; Wand, A. J. High-resolution triple-resonance NMR spectroscopy of a novel calmodulin peptide complex at kilobar pressures. *J. Am. Chem. Soc.* **1996**, *118* (45), 11329–11330.
- (32) Akasaka, K.; Yamada, H.; Inoue, K.; Herrmann, C.; Kremer, W.; Maurer, T.; Doker, R.; Kalbitzer, H. R. Pressure-induced local unfolding of the Ras binding domain of RalGDS. *Nat. Struct. Biol.* **2000**, *7* (7), 547–550.
- (33) Dumont, C.; Emilsson, T.; Gruebele, M. Reaching the protein folding speed limit with large, sub-microsecond pressure jumps. *Nat. Methods* **2009**, *6* (7), 515–U70.
- (34) Kamatari, Y. O.; Yokoyama, S.; Tachibana, H.; Akasaka, K. Pressure-jump NMR study of dissociation and association of amyloid protofibrils. *J. Mol. Biol.* **2005**, *349* (5), 916–921.
- (35) Kremer, W.; Arnold, M.; Munte, C. E.; Hartl, R.; Erlach, M. B.; Koehler, J.; Meier, A.; Kalbitzer, H. R. Pulsed Pressure Perturbations, an Extra Dimension in NMR Spectroscopy of Proteins. *J. Am. Chem. Soc.* **2011**, *133* (34), 13646–13651.
- (36) Charlier, C.; Alderson, T. R.; Courtney, J. M.; Ying, J.; Anfinrud, P.; Bax, A. Study of protein folding under native conditions by rapidly switching the hydrostatic pressure inside an NMR sample cell. *Proc. Natl. Acad. Sci. U. S. A.* **2018**, *115*, E4169–E4178.
- (37) Harper, S. M.; Neil, L. C.; Day, I. J.; Hore, P. J.; Gardner, K. H. Conformational changes in a photosensory LOV domain monitored by time-resolved NMR spectroscopy. *J. Am. Chem. Soc.* **2004**, *126* (11), 3390–3391.
- (38) Alderson, T. R.; Charlier, C.; Torchia, D. A.; Anfinrud, P.; Bax, A. Monitoring Hydrogen Exchange During Protein Folding by Fast Pressure Jump NMR Spectroscopy. *J. Am. Chem. Soc.* **2017**, *139* (32), 11036–11039.
- (39) Krantz, B. A.; Sosnick, T. R. Distinguishing between two-state and three-state models for ubiquitin folding. *Biochemistry* **2000**, *39* (38), 11696–11701.
- (40) Khorasanizadeh, S.; Peters, I. D.; Butt, T. R.; Roder, H. Folding and Stability of a Tryptophan-Containing Mutant of Ubiquitin. *Biochemistry* **1993**, *32* (27), 7054–7063.
- (41) Larios, E.; Li, J. S.; Schulten, K.; Kihara, H.; Gruebele, M. Multiple probes reveal a native-like intermediate during low-temperature refolding of ubiquitin. *J. Mol. Biol.* **2004**, *340* (1), 115–125.
- (42) Herberhold, H.; Winter, R. Temperature- and pressure-induced unfolding and refolding of ubiquitin: A static and kinetic Fourier transform infrared spectroscopy study. *Biochemistry* **2002**, *41* (7), 2396–2401.
- (43) Sosnick, T. R.; Dothager, R. S.; Krantz, B. A. Differences in the folding transition state of ubiquitin indicated by phi and psi analyses. *Proc. Natl. Acad. Sci. U. S. A.* **2004**, *101* (50), 17377–17382.
- (44) Rea, A. M.; Simpson, E. R.; Meldrum, J. K.; Williams, H. E. L.; Searle, M. S. Aromatic Residues Engineered into the beta-Turn Nucleation Site of Ubiquitin Lead to a Complex Folding Landscape, Non-Native Side-Chain Interactions, and Kinetic Traps. *Biochemistry* **2008**, *47* (48), 12910–12922.
- (45) Vallee-Belisle, A.; Michnick, S. W. Multiple tryptophan probes reveal that ubiquitin folds via a late misfolded intermediate. *J. Mol. Biol.* **2007**, *374* (3), 791–805.
- (46) Piana, S.; Lindorff-Larsen, K.; Shaw, D. E. Atomic-level description of ubiquitin folding. *Proc. Natl. Acad. Sci. U. S. A.* **2013**, *110* (15), 5915–5920.
- (47) Vajpai, N.; Nisius, L.; Wiktor, M.; Grzesiek, S. High-pressure NMR reveals close similarity between cold and alcohol protein denaturation in ubiquitin. *Proc. Natl. Acad. Sci. U. S. A.* **2013**, *110* (5), E368–E376.
- (48) Reddy, G.; Thirumalai, D. Collapse Precedes Folding in Denaturant-Dependent Assembly of Ubiquitin. *J. Phys. Chem. B* **2017**, *121* (5), 995–1009.
- (49) Reddy, G.; Thirumalai, D. Dissecting Ubiquitin Folding Using the Self-Organized Polymer Model. *J. Phys. Chem. B* **2015**, *119* (34), 11358–11370.
- (50) Khorasanizadeh, S.; Peters, I. D.; Roder, H. Evidence for a three-state model of protein folding from kinetic analysis of ubiquitin variants with altered core residues. *Nat. Struct. Biol.* **1996**, *3* (2), 193–205.
- (51) Went, H. M.; Benitez-Cardoza, C. G.; Jackson, S. E. Is an intermediate state populated on the folding pathway of ubiquitin? *FEBS Lett.* **2004**, *567* (2–3), 333–338.
- (52) Charlier, C.; Courtney, J. M.; Alderson, T. R.; Anfinrud, P.; Bax, A. Monitoring N-15 Chemical Shifts During Protein Folding by Pressure-Jump NMR. *J. Am. Chem. Soc.* **2018**, *140* (26), 8096–8099.
- (53) Erlach, M. B.; Koehler, J.; Crusca, E.; Kremer, W.; Munte, C. E.; Kalbitzer, H. R. Pressure dependence of backbone chemical shifts in the model peptides Ac-Gly-Gly-Xxx-Ala-NH₂. *J. Biomol. NMR* **2016**, *65* (2), 65–77.
- (54) Bax, A.; Pochapsky, S. S. Optimized Recording of Heteronuclear Multidimensional Nmr- Spectra Using Pulsed Field Gradients. *J. Magn. Reson.* **1992**, *99* (3), 638–643.
- (55) Keele, J.; Clowes, R. T.; Davis, A. L.; Laue, E. D. Pulsed-Field Gradients - Theory and Practice. *Methods Enzymol.* **1994**, *239*, 145–207.
- (56) Bax, A.; Ikura, M.; Kay, L. E.; Torchia, D. A.; Tschudin, R. Comparison of different modes of two-dimensional reverse-correlation NMR for the study of proteins. *J. Magn. Reson.* **1990**, *86*, 304–318.
- (57) Ikura, M.; Kay, L. E.; Bax, A. A novel approach for sequential assignment of ¹H, ¹³C, and ¹⁵N spectra of larger proteins: heteronuclear triple-resonance three-dimensional NMR spectroscopy. application to calmodulin. *Biochemistry* **1990**, *29* (19), 4659–4667.
- (58) Kiefhaber, T. Kinetic traps in lysozyme folding. *Proc. Natl. Acad. Sci. U. S. A.* **1995**, *92* (20), 9029–9033.

(59) de Dios, A. C.; Pearson, J. G.; Oldfield, E. Secondary and tertiary structural effects on protein NMR chemical shifts - an ab initio approach. *Science* **1993**, *260* (5113), 1491–1496.

(60) Peterson, R. W.; Wand, A. J. Self-contained high-pressure cell, apparatus, and procedure for the preparation of encapsulated proteins dissolved in low viscosity fluids for nuclear magnetic resonance spectroscopy. *Rev. Sci. Instrum.* **2005**, *76* (9), 094101.

(61) Delaglio, F.; Grzesiek, S.; Vuister, G. W.; Zhu, G.; Pfeifer, J.; Bax, A. NMRpipe - a multidimensional spectral processing system based on Unix pipes. *J. Biomol. NMR* **1995**, *6* (3), 277–293.

(62) Lee, W.; Tonelli, M.; Markley, J. L. NMRFAM-SPARKY: enhanced software for biomolecular NMR spectroscopy. *Bioinformatics* **2015**, *31* (8), 1325–1327.

(63) Nielsen, J. T.; Mulder, F. A. A. POTENCI: prediction of temperature, neighbor and pH-corrected chemical shifts for intrinsically disordered proteins. *J. Biomol. NMR* **2018**, *70*, 141–175.